Blind lattice parameter determination of cubic and tetragonal phases with high accuracy using a single EBSD pattern

Authors

Ming Han[a1]*, Chen Chen[a2], Guangming Zhao[ba3], Lili Li[ca], Gert Nolze[d], Baojun Yu[e], Xiaodong Huang[a] and Ye Zhu[b]*

[a]School of Materials Science and Engineering, East China Jiaotong University, Nanchang, Jiangxi, 330013, People's Republic of China

[b]Department of Applied Physics, The Hong Kong Polytechnic University, Hung Hom, Kowloon, Hong Kong, People's Republic of China

[c]School of Engineering, RMIT University, Bundoora, VIC, 3083, Australia

[d] Federal Institute for Materials Research and Testing (BAM), Unter den Eichen 87, Berlin, 12205, Germany

[e] Bruker Nano Analytics Division, No. 418 Guiping Road, Shanghai, 200233, People's Republic of China

Correspondence email: mhancn@yahoo.com; yezhu@polyu.edu.hk

[1]These authors contributed equally to this work.

[2]These authors contributed equally to this work.

[3]These authors contributed equally to this work.

Funding information Natural Science Foundation of China (grant No. 51071125); Major Project of Natural Science Foundation of Jiangxi Province (grant No. 20161ACB20010); the Hong Kong Research Grants Council through the Early Career Scheme (grant No. 25301617); the Hong Kong Polytechnic University (grant No. 1-ZE6G).

Synopsis We propose a reliable method which can accurately derive the Bravais-lattice type and its lattice parameters of unknown phases from a single EBSD pattern without *a priori* knowledge. By solving the geometric relationships in an EBSD pattern based on a huge overdetermined system of equations, error accumulation can be avoided, with the relative errors confined to ~1% for lattice parameters, <0.4% for axial ratios, and ~0.1° for crystal orientation.

Abstract The Bravais lattices and their lattice parameters are blindly determined using electron backscatter diffraction (EBSD) patterns of materials with cubic or tetragonal crystal structures. Since the geometric relationships in a single EBSD pattern are overdetermined, the relative errors of determining the lattice parameters as well as the axial ratios are confined to about (0.7±0.4)% and (0.07±0.03)%, respectively, for ideal simulated EBSD patterns. The accuracy of the crystal orientation determination reaches about 0.06°±0.03°. With careful manual band detection, the accuracy of determining experimental patterns could be comparable to those of determining simulated ones, though the latter are often better than the former which have worse pattern quality as well as uncertain systematic errors. The reasonably high accuracy is obtained primarily because the detection of the diffracting-plane traces and zone axes is relatively accurate. Our results demonstrate that the developed procedure based on the EBSD technique presents a reliable tool for crystallographic characterization of the Bravais lattices of unknown phases.

Keywords: electron backscatter diffraction; EBSD; Bravais lattice; lattice parameter; Kikuchi pattern

1. Introduction

Lattice parameters, which define the size and shape of the unit cells, are commonly used to identify or distinguish between crystalline phases. As the most effective way to determine lattice parameters, X-ray diffraction can achieve a high accuracy in the scale of 10^{-5} Å (with the relative error around 0.0005%) for perfect crystals and a single phase (Cullity, 1956). However, in case of a too little phase fraction the X-ray diffraction signal may not be sufficient; hence electron diffraction in transmission electron microscope (TEM) is a popular alternative way. The standard technique is selected area electron diffraction (SAED), and its accuracy in lattice parameter determination may reach even 10%. For the determination of unknown phases, SAED is not really suitable since too many solutions or results exist if the lattice parameters are not better determined than ±10%. Despite this comparatively big error, electron diffraction still enables the discrimination of possible phase candidates in many circumstances. The major disadvantage of electron diffraction in TEM is the process of thinning samples to be electron transparent, which can be time-consuming and even challenging. Besides, not everywhere a TEM is available.

Previously, we proposed that electron backscatter diffraction (EBSD) in a scanning electron microscope (SEM) can also be a powerful tool to determine lattice parameters. As a widespread characterization technique nowadays, EBSD enables a comprehensive microstructural characterization of crystalline materials based on both phase differentiation and derived

orientation information, i.e., in these cases the phases are known and only need to be differentiated. However, the traditional way to determine lattice parameters using EBSD has two drawbacks. The first one is that it heavily depends on the prior information of sample composition and possible phase candidates. It requires that chemical information combined with the interplanar angles (derived from visible Kikuchi bands and the source point of signals) is sufficient to recognize the correct phase from a database like the Inorganic Crystal Structure Database (ICSD). Such recognization process (i.e., searching and grouping results) may deliver tens or hundreds of possible candidates equally fulfilling the requested conditions which include possible errors in the chemical composition determination by energy-dispersive X-ray spectroscopy and the approximate lattice parameter sensitivity of EBSD. If the database search is not successful, any further measurement using EBSD for the lattice parameter determination is highly speculative. In order to improve the EBSD technique for identification of completely unknown phases, Dingley & Wright (Dingley & Wright, 2009) proposed a different way to reconstruct a three-dimensional primitive cell in reciprocal space from an EBSD pattern. Their proposed way uses the symmetric characteristics exhibited by the Kikuchi bands to improve the accuracy of the primitive cell parameters. Overall, determination of the Bravais lattice parameters cannot be accomplished through the traditional way using EBSD without significant *a priori* knowledge.

The second drawback of the traditional way lies in the fact that, even for the known phase (from a database), determining the lattice parameters using EBSD still suffers large errors (5-20%) (Goehner & Michael, 1996, Dingley & Wright, 2009). Reasonable applications of EBSD for lattice parameter determination are limited to semiconductor materials forming high-quality Kikuchi patterns (Goehner & Michael, 1996, Dingley & Wright, 2009). Even in such experimentally good cases or in dynamically simulated EBSD patterns, most Kikuchi bands do not show well-defined, sharp edges which are necessary for an accurate description of the Bragg angles and the corresponding lattice-plane spacings. The second drawback is sort of intrinsic: Already indicated by a simple two-beam approximation using the dynamical theory of electron diffraction, a band edge always shows a diffuse profile with the Bragg-angle position somewhere between the minimum and the maximum intensity (Reimer, 1998). This uncertainty of the Bragg angle position depends on the chemical and crystallographic characters of a phase. Therefore, the common conclusion is that even for the mainly investigated cubic phases the only lattice parameter a is assumed to have at best an error of ±10% like SAED.

In our previous work, we demonstrated that abundant crystallographic information provided by a single EBSD pattern can be utilized to build a huge overdetermined system of equations, the least-squares solution of which can prevent error accumulation when determining the lattice parameters. To be specific, in an EBSD pattern tens of Kikuchi bands represent the diffraction signals of lattice planes $(hkl)_i$. These Kikuchi bands intersect each other, forming hundreds of zone axes $[uvw]_m$. The connection between two intersection points of traces defines the trace of a new lattice plane whose intersections with other traces indicate other lattice directions again. This is valid for any crystal symmetry, orientation or diffraction-source position (projection center). With the precise measurement of the corresponding plane spacings and angles in between, we have thousands of equations to solve the six lattice parameters together with the crystal orientation. This abundant and interrelated crystallographic information can be used to minimize the error caused by measuring the positions and widths of Kikuchi bands, thus surpassing the second drawback. It further enables our method to determine the lattice parameters of unknown phases without *a priori* knowledge, just using a single EBSD pattern, which thus eliminates the first drawback (Li *et al.*, 2014, Li & Han, 2015). On the other hand, the accuracy of lattice parameter determination by this method has not yet been quantitatively investigated.

The present paper examines the accuracy question. To avoid uncertainties (e.g., electron wavelength, real lattice parameter and projection-center position) in experimental patterns and better evaluate the accuracy, we first apply our method on simulated EBSD patterns of different cubic phases using dynamical theory of electron diffraction, and analyze them as the simplest case of unknown phases. In the second step, the complexity has been increased by analyzing some patterns of tetragonal phases. Lastly, we examine experimental EBSD patterns and derive the accuracy. Effects from main experimental conditions (e.g., pattern resolution, electron wavelength, etc.) on the accuracy are also investigated. The derived errors are ~1% for lattice parameters, <0.4% for axial ratios, and ~0.1° for crystal orientation determination. The high accuracy determined in our work, combined with other advantages of the EBSD including its wide accessibility in SEM, simple sample preparation and data acquisition, further demonstrates that EBSD technique is a promising tool for crystallographic characterization of unknown phases.

2. Applied procedure

The derivation of the Bravais lattice parameters from a single Kikuchi pattern is developed in a software called *EBSDL* (Li *et al.*, 2014). It takes into account that each zone axis $[uvw]$ is described by

$$\vec{R} = u\vec{a} + v\vec{b} + w\vec{c} \tag{1}$$

where $\vec{a}$, $\vec{b}$, $\vec{c}$ are the basis vectors of the Bravais lattice in real space. In contrast, the normal of a diffracting plane (hkl) is defined by

$$\vec{H} = h\vec{a}^* + k\vec{b}^* + l\vec{c}^* \tag{2}$$

where $\vec{a}^*$, $\vec{b}^*$, $\vec{c}^*$ are the basis vectors of the reciprocal lattice. Their higher-order interferences *hkl* are given by a vector with the same direction as (hkl), however, they have a longer (inverse) length according to their order *n*. The correlation between band width and reciprocal lattice point *hkl* is given by Bragg's equation:

$$n\lambda = 2d_{(hkl)} \sin\theta \tag{3}$$

It can also be described as

$$\frac{\lambda}{2}\left|\vec{H}_i\right| = \sin\theta_i \approx \theta_i \tag{4}$$

Hence, the length of the reciprocal lattice vector *hkl* is proportional to the band width (Nolze & Winkelmann, 2017):

$$\left|\vec{H}_i\right| \propto \theta_i \tag{5}$$

In order to reduce errors, *EBSDL* considers as many as possible zone axes $[uvw]_i$ defined by multiple intersecting lattice planes $(hkl)_j$. Because of reciprocity, each zone axis $[uvw]_i$ as a lattice vector also represents a lattice plane $[uvw]_i^*$ in the reciprocal space consisting of at least two reciprocal lattice vectors hkl_j which must fulfill the condition: $u_i h_j + v_i k_j + w_i l_j = 0$. From the two vectors hkl_1 and hkl_2, all other hkl_j in this plane can be derived by a simple linear combination

$$hkl_j = m_1 \cdot hkl_1 + m_2 \cdot hkl_2 \quad (m_1, m_2, \text{ integers}) \tag{6}$$

where hkl_1 and hkl_2 are the shortest vectors and represent the basis vectors for this reciprocal lattice plane $[uvw]_1^*$. Simultaneously, each hkl_j is also part of at least another zone $[uvw]_2$, so that this vector also needs to match to the two-dimensional lattice of a reciprocal lattice plane $[uvw]_2^*$. It should be noticed that for a proper use of the respective zone axes $[uvw]_i$, they have

to be rotated virtually into the so-called pattern center which is identical to the center of the gnomonic projection. Only then the angles between the diffracting lattice planes are identical to the angles between their traces. Fig. 1 illustrates this fundamental concept of *EBSDL*. For simplicity, only nine Kikuchi bands (numbered as 1 to 9) are considered and only five from ten visible zone axes are labelled (by B to F) in Fig. 1a. Moving $[uvw]_i$ into the pattern center, the normal direction to each trace of the diffracting $(hkl)_j$ is then parallel to the respective reciprocal lattice direction *hkl* in the reciprocal lattice plane $[uvw]^*$. The width of the band is proportional to the length of the reciprocal lattice vector *hkl*.

In Fig. 1b, for example, the zone of B is described as a reciprocal lattice plane. Three bands pass the zone axis B, i.e., three reciprocal lattice vectors (solid lines) follow with strong restraints: First, their directions are defined by the normals to the trace of the diffracting lattice planes, and second, their lengths unequivocally defined by their band widths. According to Eq. (6), from two reciprocal vectors, the third as well as any other reciprocal lattice vector (if any) of this zone are pinpointed. Their positions (i.e., for the reciprocal lattice points) are defined by the intersections of the regularly dashed lines in a reciprocal lattice plane (Fig. 1b). Each reciprocal lattice vector *hkl* derived from a visible band (or its different orders of interferences) belonging to the same zone must match to one of the intersection points. Similarly, Figs. 1c–1f correspond to the zone axes C–F and associated Kikuchi bands, respectively. Since the zone axes in a crystal lattice are not independent, the reciprocal lattice planes (Figs. 1b–1f) are not independent either. It turns out that only a very small number of bands and their widths can fix the positions and widths of all other bands (Nolze & Winkelmann, 2017). The redundant information from all bands can be used to increase confidence by minimizing the deviation and thus determines the least-squares solution. Comparing the large amount of Kikuchi bands and zone axes with the very limited number of primitive cell parameters (in maximum 6 independent variables) and the unknown orientation (3 Euler angles), the over-determination of the equation system becomes obvious. Its least-squares solution determines the primitive cell parameters. A detailed description of *EBSDL* is given in references (Li *et al.*, 2014, Li & Han, 2015).

An EBSD pattern contains lots of uncertainties which will affect the accuracy of lattice parameter determination. Essential experimental parameters such as projection center and electron wavelength may deviate from their true values, which influences the accuracy and precision of the derived lattice parameters. Furthermore, other factors induce errors too, such

as image distortions, high noise level in experimental patterns, and asymmetric band profiles due to excess/deficiency caused by the high sample tilt. The present paper first focuses on the errors caused exclusively by the band definition (of positions and widths) stated above. To this end, simulated EBSD patterns are used and generated with the software DynamicS (Bruker-Nano) (Winkelmann *et al.*, 2007). For the purpose of investigating the accuracy of both lattice parameters (absolute size) and lattice-parameter ratios (relative size), five cubic and five tetragonal phases are chosen. The accuracy and precision of the lattice-parameter ratio *c/a*, which mainly depends on zone-axis positions, are tested using the tetragonal phases only. The crystal structure descriptions of the ten different phases used for simulations in DynamicS are given in references (Paton & MacDonald, 1957, Otte, 1961, Wyckoff, 1963, Trojer, 1966, Robinson *et al.*, 1971, Wilburn & Bassett, 1978, Howard *et al.*, 1991, Bideaux *et al.*, 1995, Swope *et al.*, 1995). In addition, three Euler angles representing the crystal orientation (in Z-X-Z Bunge notation) as well as the essential experimental parameters, are arbitrarily chosen for simulating the EBSD pattern of each phase. Then the simulated patterns are analyzed by the program *EBSDL* which is the only tool we use to treat the input patterns as from completely unknown phases and to perform the determination of their lattice parameters and crystal orientations. This enables us to have not only a definite projection center and electron wavelength for our analysis, but also reference lattice parameters and crystal orientations for error determination. In practical applications, the experimental parameters are important and hence they will also be discussed in detail afterwards.

3. Results and discussion

Fig. 2a shows one of the simulated EBSD patterns of a cubic phase. Green lines mark the virtual traces of 65 visible diffracting but unknown lattice planes $(hkl)_i$. Red circles indicate 395 intersections and represent unknown zone axes $[uvw]_j$. A yellow cross denotes the position of the pattern center. Since the widths of Kikuchi bands decide the absolute value of lattice parameters, manual identification of the band edges is the most essential step during the whole process of lattice-parameter determination and Bravais-lattice derivation. However, band-edge description of the interweaved Kikuchi bands is challenging. For instance, owing to the existence of higher-order interferences, some diffraction orders of the band (marked by two black arrows in Fig. 2a) have sharp edges. The first-order, however, is even theoretically blurred (Reimer, 1998). It is marked by two white arrows and represents exactly 1/8 of the width of the band marked by black arrows, i.e., the black arrows indicate the eight-order

interference at this lattice plane. The band-edge description is further aggravated by the fact that all edges are mathematically defined by hyperbola (conic sections) where the pattern center defines the shared central point. Since the hyperbolic deviation becomes dominant with increasing distance to the pattern center, these areas react very sensitive on unsuitable band-edge descriptions. If the band edges in these sensitive areas of an EBSD pattern were well-described, in other areas the visible band edges and the described hyperbolas will show the lowest discrepancy. This feature is essential for an accurate lattice parameter determination. For example, in the four corners of Fig. 2a, deviations preferably arise between the straight lines used during band-width selection and the real-hyperbolic shape of the band edge. Therefore, such sensitive areas can be defined, where red lines show the calculated hyperbolas for the assumed projection center. It is apparent that the red hyperbola segments show a convincing correlation to the corresponding Kikuchi-band edges. It needs to be pointed out that the measurement of each band width is an independent process so that each band width is characterized by a measurement error. Specifically, the measurement error of the Bragg-angle positioning can be expressed by $\theta - \theta_B$, where θ_B is the true Bragg-angle position and θ is the measured one. Only when all trace positions (rectilinear band centers) and Bragg-angle positions (hyperbolic band edges) are well-described, the band definition process is completed and finally a reliable result with high accuracy can be expected. The major assumption is that the manual definition of all band widths scatters around the true values so that the applied least-squares refinement for all bands and zone axes results in the derived lattice parameters close to the true ones.

For the Kikuchi pattern in Fig. 2a the results are given in Table 1. The corresponding phase is sulvanite (Cu_3VS_4) which is described by a primitive cubic lattice (a = 5.3912 Å (Trojer, 1966)). The derived lattice parameter is a = 5.419 Å, with an error below 1%, as shown in Table 1. This indicates that our band-width measurement error is less than 1/100 of the band widths, which is excellent. Since the projection center is known, the other free parameter is the crystal orientation following from the defined Bravais-lattice description. The derived crystal orientation defined by the Euler angles is (5.01°, −20.02°, 30.05°), with the average error between the input and derived three Euler angles ~0.03°.

Similarly, Fig. 2b shows a determined EBSD pattern of a phase described by the tetragonal lattice. Other eight phases with cubic and tetragonal crystal lattices are also analyzed using single EBSD pattern of each phase, and their Bravais lattices and lattice parameters are determined as unknown phases. The results of all evaluated phases are summarized in Table 1,

which lists the derived Bravais lattice, the lattice parameters, the lattice-parameter ratio, the crystal orientation (Euler angles), as well as the corresponding errors.

It is evident from Table 1 that, for simulated patterns under the condition of no experimental errors (such as uncertain sample geometry, energy divergence of electron beam, lens distortions and signal-to-noise limitations in the EBSD camera, etc.), the relative errors of the determined lattice parameters and *c/a* ratios are about (0.7±0.4)% and (0.07±0.03)%, respectively. The accuracy of the crystal orientation determination is about 0.06°±0.03°.

After evaluating errors using simulated EBSD patterns, we next examine the lattice-parameter determination error from experimental patterns. Compared to simulated patterns, the quality of experimental patterns should be worse: most band edges appear highly blurred; many bands (or rather hyperbola segments) are only distinguishable in local regions. The worse quality of experimental patterns should lead to larger errors in lattice-parameter determination.

Fig. 3a shows a determined experimental pattern of ferrite. In total, 80 bands and 527 zone axes are properly detected. The determination results are also given in Table 1. Since the exact lattice parameters of ferrite for the experimental pattern (Fig. 3a) are unknown, which depend on the material composition, internal stress, etc., we take the published structure as a reference for lattice parameters (Wilburn & Bassett, 1978). To justify our choice of reference, we first simulate an EBSD pattern using the published structure (Fig. S1a), and compare with the experimental pattern in Fig. 3a. The cross correlation between Fig. 3a and Fig. S1a is 0.8 which indicates a good coincidence and validates our choice of reference. Consequently, the errors of determining the experimental pattern of ferrite are 1.08% (for *a*) and 0.44° (for Euler angles). Similarly, Fig. 3b is a determined experimental pattern of rutile. Fig. S1b is corresponding simulated pattern again using published structure (Swope *et al.*, 1995) with the same orientation as Fig. 3b. The cross correlation between Fig. 3b and Fig. S1b is 0.6. The determination results as well as corresponding errors are also given in Table 1. The results demonstrate that the accuracies of determining simulated and experimental patterns are comparable, though the latter is inevitably worse due to the degraded pattern quality as well as uncertain systematic errors.

In order to further elucidate the effects of the main experimental factors (i.e., pattern resolution, electron wavelength, detector distance) on the determination accuracy of lattice parameters, we vary one of them while keeping the others constant, and perform a series of independent determinations applied on the same phase with cubic or tetragonal crystal lattice. In addition, for a simply practical reason, namely, the manual band definition is pixel-related

(Wright *et al.*, 2015), we also investigate the potential effect of the screen resolution on the accuracy and precision.

Fig. 4a displays the impact of the pattern resolution using a Kikuchi pattern of sulvanite (Cu_3VS_4, cubic). Other factors, such as screen resolution (3840 × 2160 pixels), electron wavelength (assuming an electron energy E = 20 keV), detector distance (1.0, i.e. the ratio between the crystal-to-detector distance and the vertical detector dimension is equal to 1), and a non-rotated crystal with Euler angles (0°, 0°, 0°) (i.e., the normal to the plane of the EBSD pattern is ⟨1 0 0⟩) are kept constant. The relative lattice-parameter error $\left|a - a_0\right| / a_0 \times 100\%$ (lower ordinate) refers to the used value of a_0 = 5.3912 Å (Trojer, 1966). The upper ordinate describes the average misorientation angle between the input Euler angles (0°, 0°, 0°) for pattern simulation and the derived three angles (Z, X, Z), cf. Table 1. Both the lattice-parameter errors and the misorientation angles in Fig. 4a are average values of several independent measurements. The diagram shows that with increasing pattern resolution the lattice-parameter error decreases as represented by a dotted-line arrow. This is because the increased resolution of the EBSD pattern makes its features more visible. As for the misorientation angle (upper ordinate), it is very small (< 0.1°), which reaches the limit of the EBSD method reported in this paper. The decreasing trend of the lattice-parameter error does not mean that it will endlessly decrease only by increasing the Kikuchi-pattern resolution.

The diagram in Fig. 4b displays the effect of the screen resolution. Other factors and testing conditions are the same as used for Fig. 4a, except for the Kikuchi-pattern resolution which is now fixed as 1084 × 1084 pixels. Since positioning and measuring of the Kikuchi bands and widths are pixel-dependent, a high screen resolution enables not only a better zooming of the highly-resolved EBSD pattern without considerably fuzzing the pattern, but also a better positioning and measuring of the Bragg angles and band widths in the subpixel scale. Consequently, the uncertainty $\theta - \theta_B$ could be improved, and hence the Kikuchi bands and zone axes in the same EBSD pattern could be defined more accurately with higher screen resolution. This conclusion is supported by Fig. 4b, in which the lattice-parameter error continuously decreases with increasing screen resolution.

Similarly, the diagram Fig. 4c displays the effect of the accelerating voltage. Considering the relativistic effects, electron wavelength is given by $\lambda = h \Big/ \left[2m_0 E \left(1 + E/2m_0 c^2 \right) \right]^{1/2}$, where h designates Planck's quantum of action, m_0 the rest mass of an electron, E the kinetic energy of the electron, and c the speed of light in vacuum. As the accelerating voltage increases

(electron wavelength decreases with $1/\sqrt{E}$), every Kikuchi band of the same material becomes narrower. Considering the decreasing number of pixels, measurement of the band widths becomes less precise, which leads to the increased determination errors (Fig. 4c).

Fig. 4d displays the impact of the detector distance. The detector distance is a flexible experimental parameter for obtaining wide or narrow Kikuchi bands, which affects the relative error of band-width measurement. As the detector distance increases, the resulting EBSD patterns have similar effect to that induced by increasing pattern resolution. The lattice-parameter errors at detector distance 0.6 and 0.8 are apparently larger than those at 1.0, 1.2, and 1.4, although the errors in Fig. 4d do not show a clear tendency which is possibly because the determination accuracy reported in this paper has already reached its limit and thus the derived result scatters near its accuracy limit.

For the tetragonal zircon ($ZrSiO_4$), Fig. 5 displays the effects of the same set of influencing factors. The error trends are comparable to those displayed in Fig. 4. A noticeable feature of Fig. 5 is the lattice-parameter ratio *c/a*. Like the misorientation angle (< 0.1°) in Fig. 4 and Fig. 5, the error in *c/a* (< 0.5%) is very small, too. This is due to the fact that both crystal orientation and *c/a* axial ratio are directly related to the zone-axis positions. The accuracy of zone-axis positions is clearly higher than that of the Kikuchi-band widths which are only necessary to determine the absolute size of the lattice parameters.

Apart from the four influencing factors discussed above, two further factors also considerably affect the determination errors, namely, the projection center and the number of bands used. Firstly, a variation of the projection-center position changes the reference directions and hence all three-dimensional directions of the zone axes will be changed accordingly. This affects everything, i.e. lattice parameters, axial ratio, and crystal orientation. However, since *EBSDL* is able to refine the position of the projection center according to both the positions of zone axes and the widths of Kikuchi bands, the impact of the projection center is not discussed in this paper. Secondly, for statistical reasons, the number of describable Kikuchi bands is critical. We note that if the bands with the narrowest width (lowest interference order) were incorrectly defined or even not described at all, the derived Bravais lattice of the unknown phase might be wrong or cannot be discovered since the derived reciprocal vectors are inconsistent to other zone axes. This is because narrow bands reflect short reciprocal lattice vectors which might be the basis vectors of the reciprocal lattice, cf. Fig. 1.

Fortunately, additional simple relationship exists and can help to discover the

inconsistencies. For example, for a given crystal the volume of its three-dimensional primitive cell is unique. Since it contains a single lattice point, non-primitive cells with more than one lattice points have an integral multiple of the volume of the primitive cell. Additionally, selection of the shortest reciprocal vectors simplifies definition of the primitive unit cell and enables recognition of the correct Bravais lattice.

As the determination of cubic or tetragonal Bravais lattice is performed using only diffraction geometry information obtained from a single EBSD pattern (e.g., its zone-axis positions and Kikuchi-band widths), the applied procedure in this study is completely independent of crystal symmetry and therefore applicable to all crystal systems (Li & Han, 2015). The lattice-parameter ratios (b/a, c/a) and inter-axial angles (α, β, γ) and hence corresponding possible Bravais-lattice type can be decided by solving an over-determined system of equations based on zone-axis positions and their crystallographically interrelated angles (Li *et al.*, 2014). Despite its wide applicability, accurate determination of lattice parameters via the EBSD technique requires a high pattern quality, i.e., having many clearly visible Kikuchi bands with sharp edges. However, obtaining such high-quality EBSD patterns is sometimes quite challenging. For example, some materials of low-Z elements usually produce weak diffraction signals; some non-cubic crystalline materials with complex crystal structures also have the visibility of most Kikuchi band edges weakened; still others may be accompanied by relatively poor crystalline perfection or fine grain size, making their specimen preparation difficult and even no patterns achievable at last. In light of the challenges to obtaining high-quality EBSD patterns, further investigations regarding low-Z, low-symmetry, or high-structure-complexity materials need to be carried out in the future.

4. Summary and conclusion

We investigate the simulated EBSD patterns of ten cubic or tetragonal phases in order to evaluate the accuracy of their lattice parameters which are derived from a single EBSD pattern of each phase. The relative errors of the lattice parameters and the lattice-parameter ratios are about (0.7±0.4)% and (0.07±0.03)%, respectively. The accuracy of the average misorientation angle between theoretical and experimentally derived Euler angles is about 0.06°±0.03°. Such reasonably high accuracy is obtained under ideal conditions (e.g., high resolution, exactly known projection center, and no noise) and is the best result of our proposed procedure so far. The high accuracy of determining unknown Bravais lattices from a single Kikuchi pattern can be obtained because of different reasons:

a) The relationship between lattice planes $(hkl)_i$ and lattice directions $[uvw]_j$ is fully applied to define the traces and intersection points of the lattice planes. It is a collective description, i.e., if three traces of non-tautozonal $(hkl)_i$ are correct, all other traces are correct as well. In other words, the detection of the diffracting-plane traces and zone axes is relatively accurate, which is prerequisite to an accurate determination of the lattice parameters and crystal orientation.

b) Using hundreds of zone axes $[uvw]_j$, a huge over-determined equation system generally comprising tens of thousands of equations can be built according to the angles between those zone axes. The least-squares solution of this equation system gives an accurate axial ratio. The *absolute* lattice parameters can be further refined by the widths of Kikuchi bands.

c) As done for the band-trace definition, also the band widths are manually defined. The applied Hough transform still has a lower accuracy compared to the manual detection. A further implementation of multiple reflection orders may further improve accuracy and precision (Fig. 2a).

For actual experimental patterns, they suffer from more errors, such as uncertain sample geometry, energy divergence of electron beam, lens distortions and signal-to-noise limitations in the EBSD camera, etc. These errors will affect the ultimate lattice parameter measurement resolution that can be achieved. Nevertheless, with careful manual band detection, the accuracy and precision of determining experimental patterns could be comparable to those of determining simulated ones, though the latter are inevitably better. In addition, any enhancement in pattern quality, such as by applying image processing techniques or adopting high-sensitivity EBSD detectors, will certainly be beneficial to the determination accuracy.

Although the reported accuracy is reasonably high, the determination process is still time-consuming because of the widely manual definition of the band positions and widths. Despite this shortcoming, a single EBSD pattern carries numerous (though redundant) crystallographic information about the primitive cell of the unknown phase and enables further derivation of its Bravais lattice if no pseudo-symmetry exists. Future objective is to further improve the determination accuracy and processing efficiency, e.g., by using multiple-order interferences or by implementing an automatic algorithm for a more reliable Kikuchi-band definition.

In summary, our method can accurately derive both Bravais-lattice type and lattice parameters from a single EBSD pattern without any additional information. As expected many years ago, EBSD in SEM is not only a powerful tool for orientation characterization, it also

enables evaluation or identification of the crystallographic nature of the even unknown phases occurring in a material.

Figure 1 Illustrations demonstrating the fundamental principle of the applied EBSD method: a) A schematic Kikuchi pattern with nine bands (numbered as 1 to 9) and five zone axes (marked by B to F); b)–f) Derived reciprocal lattice planes containing all their reciprocal lattice vectors, which belong to the zone axes B–F shown in a), respectively.

Figure 2 Determined EBSD patterns of typical materials with (a) cubic and (b) tetragonal crystal structures.

Figure 3 Determined experimental patterns of ferrite (a) and rutile (b).

Figure 4 Effects of these EBSD parameters, a) pattern resolution, b) screen resolution, c) accelerating voltage, and d) detector distance, on the accuracy and precision of determining a cubic Bravais lattice.

Figure 5 Effects of these EBSD parameters, a) pattern resolution, b) screen resolution, c) accelerating voltage, and d) detector distance, on the accuracy and precision of determining a tetragonal Bravais lattice.

Table 1 Comparison between published (or theoretical) and determined values of ten different materials' lattice parameters and crystal orientations.

[a]Materials	[b]Bravais lattices	Published values						Determined values						Determination errors			
		a_0 (Å)	c_0 (Å)	c_0/a_0	[c]Euler (°)			a (Å)	c (Å)	c/a	Euler (°)			a (%)	c (%)	c/a (%)	[d]$\Delta Angle$ (°)
					Z_0	X_0	Z_0				Z	X	Z				
Sulvanite (Cu_3VS_4)	PC	5.3912			5	-20	30	5.419			5.01	-20.02	30.05	0.52			0.03
Austenite	FCC	3.6600			-23	-8	41	3.663			-22.91	-8.03	40.86	0.08			0.09
Copper	FCC	3.6150			-31	5	-2	3.644			-30.88	4.97	-2.09	0.80			0.08
Ferrite	BCC	2.8660			-16	59	8	2.883			-15.93	59.01	8.01	0.59			0.03
Ferrite*	BCC	2.8660			115.34	-23.96	42.19	2.835			115.88	-23.65	41.73	-1.08			0.44
Molybdenum	BCC	3.1473			-45	10	3	3.169			-45.07	9.98	3.11	0.69			0.07
Zircon ($ZrSiO_4$)	BCT	6.6070	5.9820	0.9054	-9	-34	23	6.556	5.931	0.9047	-8.97	-34.00	23.00	-0.77	-0.85	-0.08	0.01
Anatase (TiO_2)	BCT	3.7845	9.5143	2.5140	22	7	-19	3.744	9.413	2.5142	22.16	7.00	-18.95	-1.07	-1.06	0.01	0.07
Crystobalite (SiO_2)	PT	4.9717	6.9223	1.3923	17	-2	-11	4.956	6.894	1.3910	17.08	-2.02	-11.12	-0.92	-1.23	-0.09	0.07
Pinnoite ($MgB_2O(OH)_6$)	PT	7.6200	8.1900	1.0748	-37	28	-9	7.636	8.213	1.08	-36.93	28.02	-9.09	0.14	0.51	0.07	0.06
Rutile (TiO_2)	PT	4.5870	2.9540	0.6440	56	-12	0	4.591	2.959	0.6445	56.05	-12.01	-0.03	0.07	0.34	0.08	0.03
Rutile*	PT	4.5870	2.9540	0.6440	-49.26	74.33	55.59	4.586	2.942	0.6415	-49.19	74.45	55.47	-0.02	-0.41	-0.38	0.11

[a]The name of a material with an asterisk (*) means that the determination results are derived from an experimental pattern.

[b]PC, FCC, BCC, BCT and PT are abbreviations for primitive cubic, face-centered cubic, body-centered cubic, body-centered tetragonal and primitive tetragonal, respectively.

[c]The three Euler angles Z_0-X_0-Z_0 were randomly set for different materials and input into DynamicS for pattern simulation. For the materials with an asterisk (*), Z_0-X_0-Z_0 are obtained by DynamicS based on the cross correlation between experimental and corresponding simulated patterns.

[d]$\Delta Angle$ is the average misorientation angle between the input (Z_0-X_0-Z_0) and the determined (Z-X-Z) three Euler angles.

Acknowledgements The authors would like to give special thanks to Bruker Nano GmbH for providing DynamicS, the first software for Kikuchi-pattern simulation based on the dynamical theory of electron diffraction.

References

Bideaux, R. A., Bladh, K. W., Nichols, M. C. & Anthony, J. W. (1995). *Handbook of mineralogy: Silica, silicates*. USA: Mineral Data Publishing.

Cullity, B. D. (1956). *Elements of x-ray diffraction*. USA: Addison-Wesley Publishing Company, Inc.

Dingley, D. J. & Wright, S. I. (2009). *J. Appl. Cryst.* **42**, 234-241.

Goehner, R. P. & Michael, J. R. (1996). *J. Res. Natl. Inst. Stand. Technol.* **101**, 301-308.

Howard, C. J., Sabine, T. M. & Dickson, F. (1991). *Acta Crystallogr.* **B47**, 462-468.

Li, L. & Han, M. (2015). *J. Appl. Cryst.* **48**, 107-115.

Li, L., Ouyang, S., Yang, Y. & Han, M. (2014). *J. Appl. Cryst.* **47**, 1466-1468.

Nolze, G. & Winkelmann, A. (2017). *J. Appl. Cryst.* **50**, 102-119.

Otte, H. M. (1961). *J. Appl. Phys.* **32**, 1536-1546.

Paton, F. & MacDonald, S. G. G. (1957). *Acta Crystallogr.* **10**, 653-656.

Reimer, L. (1998). *Scanning electron microscopy physics of image formation and microanalysis*, Second ed. New York: Springer.

Robinson, K., Gibbs, G. V. & Ribbe, P. H. (1971). *Am. Mineral.* **56**, 782-790.

Swope, R. J., Smyth, J. R. & Larson, A. C. (1995). *Am. Mineral.* **80**, 448-453.

Trojer, F. J. (1966). *Am. Mineral.* **51**, 890-894.

Wilburn, D. R. & Bassett, W. A. (1978). *Am. Mineral.* **63**, 591-596.

Winkelmann, A., Trager-Cowan, C., Sweeney, F., Day, A. P. & Parbrook, P. (2007). *Ultramicroscopy* **107**, 414-421.

Wright, S. I., Nowell, M. M., Kloe, R., Camus, P. & Rampton, T. (2015). *Ultramicroscopy* **148**, 132-145.

Wyckoff, R. W. G. (1963). *Crystal structures*, Second ed. New York: Interscience Publishers.

Supporting information

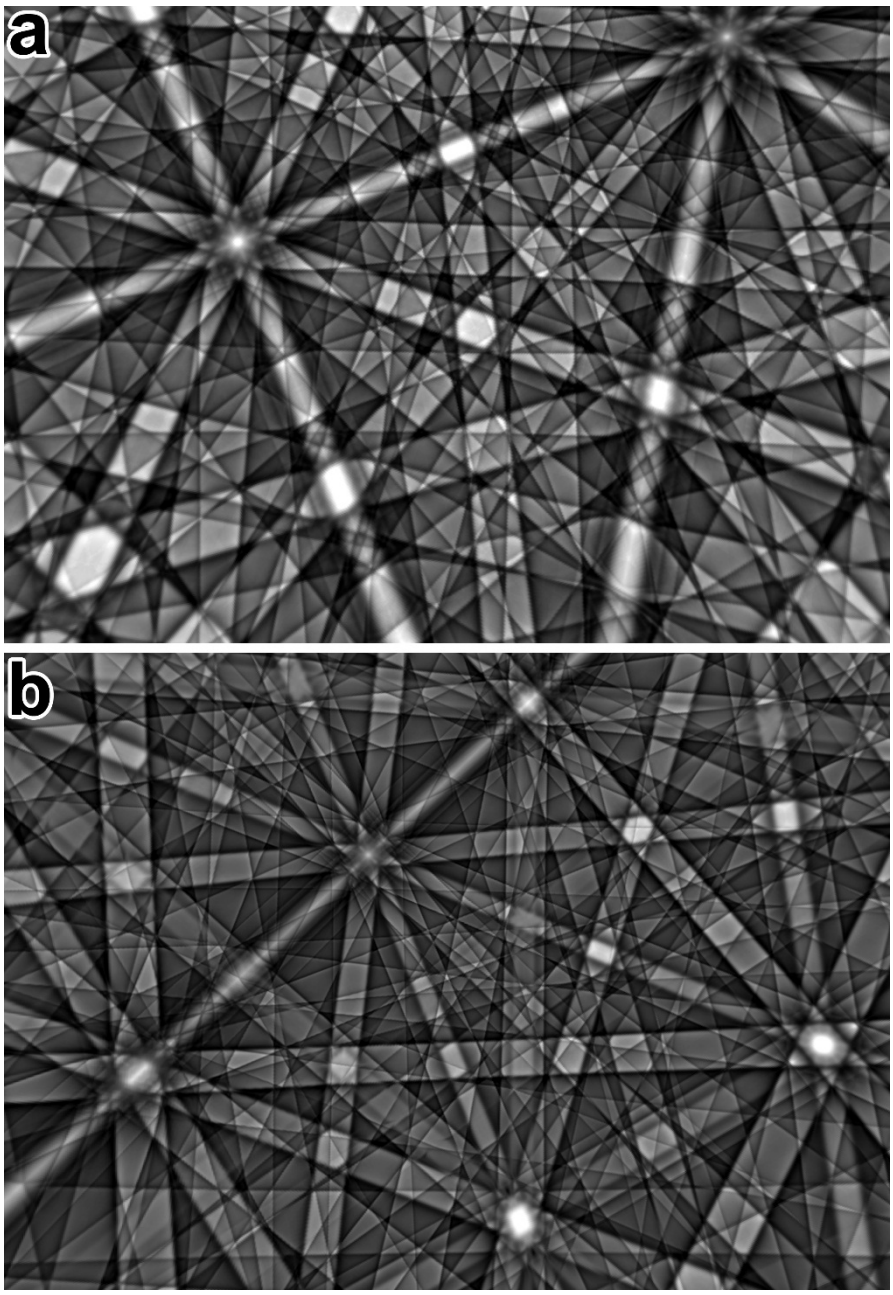

Figure S1 Simulated patterns based on the experimental patterns shown in Fig. 3: (a) ferrite and (b) rutile.